LEVEL

AD A090504

PSR Report 912

ANALYSIS OF LIDAR UTILITY FOR CHARACTERIZING BATTLEFIELD ENVIRONMENTS

May 1979

R.E. Warren
R.F. Lutomirski

Final Report
Contract No. DAAB07-78-C-2427

Sponsored by

Army Night Vision and Electro-Optics Laboratory
Fort Monmouth, New Jersey

PACIFIC-SIERRA RESEARCH CORP.
[illegible]

(1)

(14) PSR ~~REPORT~~-912

(6) ANALYSIS OF LIDAR UTILITY FOR CHARACTERIZING BATTLEFIELD ENVIRONMENTS.

(12) 52

(11) MAY 1979

(10) R. E. Warren
R. F. Lutomirski

(9) Final Report,
Contract No. DAAB07-78-C-2427
(15)

Sponsored by

Army Night Vision and Electro-Optics Laboratory
Fort Monmouth, New Jersey

PACIFIC-SIERRA RESEARCH CORP.

1456 Cloverfield Blvd. • Santa Monica, California 90404

407486

PREFACE

This report describes work performed under Contract DAAB07-78-C-2427 with the Army Night Vision and Electro-Optics Laboratory from April 1978 to May 1979.

CONTENTS

FIGURES

TABLES

SYMBOLS

Symbol	Definition
a_R	Receiver aperture radius
a_T	Transmitter aperture radius
α	Backscatter-to-extinction ratio
$\underline{b}$	Transmitter/receiver bistatic offset
β	Backscatter coefficient
β_a	Ambient backscatter
β_0	Obscurant cloud backscatter
β_T	Target reflectance
c	Speed of light
$C_g(z)$	Mass concentration (gm/cm^3)
CL	Indefinite integral of $C_g(z)$
χ	Scattering phase function
χ_T	Target scattering phase function
E(t)	Transmitter pulse shape
E_0	Transmitter pulse energy
ε	Extinction coefficient
ε_a	Ambient extinction
ε_0	Obscurant cloud extinction
f	Transmitter focal length ($\theta_T = -a_T/f$)
G_k	Green's function for kth order light
G_T	Green's function for diffuse target
γ	$1 - c(t - t')/2f$
J	Radiance
J_k	Radiance contribution of kth order light

Symbol	Definition
J_T	Target radiance
$\underline{n}$	Unit direction vector
$\underline{n}_\perp$	Transverse direction vector ($\underline{n} = (\underline{n}_\perp, n_3)$)
$\underline{n}_T$	Normal to target
$N(z)$	Number of particles/volume
$n(r,z)$	Number of particles of radius r at range z/volume
P_k	Power collected for kth order light
P_T	Target power
$\underline{r}$	Three dimensional position vector ($\underline{r} = (\underline{\rho}, z)$)
r	Particle radius
$\underline{r}_T$	Vector to target center
$\underline{\rho}$	Transverse position vector
ρ_0	Mass density of obscurant material
S_k	Source function for kth order light
σ	1/e radius of obscurant cloud
σ_{tot}	Extinction cross section
$\frac{d\sigma_a}{d\Omega}$	Differential scattering cross section
t	Time
T	Transmission of medium
T_0	Transmission of transmitter/receiver
$\underline{\theta}$	Small angle approximation to $\underline{n}_\perp$ ($\sin\theta \simeq \theta$)
θ_R	Receiver field-of-view 1/2 angle
θ_T	Transmitter beam divergence 1/2 angle
V_ρ	Volume/particle

Symbol	Definition
ξ	ct
z	Range
z_0	Range to obscurant cloud center
z_T	Range to target

1. INTRODUCTION

The use of lidar to infer information about battlefield obscurants such as smoke and dust has received considerable attention in recent years. Review articles,[1,2] feasibility studies,[3,4] and experiments[5,6] have demonstrated that state-of-the-art lidars can provide *relative* transmission and spatial concentration data for three dimensional obscurant clouds. In spite of this, the theoretical models necessary for interpreting the lidar return have not contained dependencies on all of the relevant transmitter and receiver parameters, and have been almost entirely limited to first order scatter. Since the conditions for these models to be valid are not always met, there appeared to be a need for a more fundamental theoretical basis which would reproduce the usual equations as an approximation and would give a clear basis for understanding their limitations and generalizing them as required. Providing this model was one of the primary aims of the contract.

In addition, analyses of the inversion problem have been largely qualitative and lacking in explicit mathematical algorithms for deriving information about the scattering medium from the lidar return. The work of Lamberts[7] on finding statistical correlations between the lidar return and independently observed aerosol scattering data is an exception, but it is unclear how a quasi-real time algorithm could be developed along these lines. For this reason another important aim of the contract was to derive explicit algorithms using the lidar signal either by itself or in conjunction with supporting measurements to derive information about the scattering medium.

It is essential to specify the type of information required about the obscuring medium; for tactical applications usually only the optical transmission is important. In this case it appears possible to perform a relatively simple integration of the lidar return. For field studies on the kinetics of explosive rounds, however, a detailed space-time history of the debris concentration is needed and perhaps even an estimate of particle size distributions and relative numbers of scattering constituents. These diagnostic goals are much harder to implement and either supporting local measurements of the particle scattering cross sections or use of multiple wavelengths is required in addition to the lidar signal. Part of the contract involved attempting to specify clearly what additional information would be needed to perform these additional tasks.

In section 2.1 a general solution to the radiation transport equation is obtained as an expansion in the ratio of backscattering to extinction coefficients. This is valid because computer calculations of Mie scattering for particles with refractive indices such as smoke and dust show this ratio is much less than one; thus the series converges quickly.

In section 2.2 approximations of small angle scattering and Gaussian aperture weighting functions are combined to yield the dependence of the first order backscattered power on the lidar receiver aperture size and field-of-view, as a function of time.

In section 2.3, assuming a Gaussian transmitter beam and a three dimensional density distribution for the smoke cloud, the expression developed in section 2.2 is integrated to yield an analytical expression for P_1 in terms of the parameters of the lidar system and the environmental parameters of the smoke cloud. We then introduce a model for the return from a target positioned beyond the smoke cloud and obtain the total lidar signal for the cloud-target combination. This latter model is important for assessing the ability of the smoke cloud to obscure a target.

Following an outline of our inversion approach in section 3.1 we derive an analytic expression for the path transmission as a function of the lidar signal, system constants, and backscatter-to-extinction ratio α in section 3.2.

The sensitivity of the transmission expression to noise and uncertainties in α is investigated in section 3.3 using a combination of analytical and simulation techniques. In section 3.4 we consider means of enhancing the inversion algorithm performance by additional measurements in a small region of the propagation path of scattering parameters. Finally, we outline an analytical approach for using multiple wavelengths to infer particle size distributions and concentrations in section 3.5.

Section 4 summarizes our conclusions of how well the proposed inversion techniques would perform and suggests additional work to improve the multiple wavelength approach.

2. MULTIPLE SCATTERING THROUGH A SPATIALLY VARYING TURBID MEDIUM

2.1 General Formalism

In this section we present a formal solution to the radiative transport equation for a spatially varying medium. Although the application to lidar involves predominantly single scattered radiation for smoke and dust aerosols, it is useful to base the calculations on a more general formulation that is capable of straightforward extention to other situations.

The radiative transport equation for a general scattering medium has the form

$$\frac{1}{c}\frac{\partial J}{\partial t}(\underline{r},\underline{n},t) + \underline{n}\cdot\underline{\nabla}_r\, J(\underline{r},\underline{n},t) = -\varepsilon(\underline{r},t)\, J(\underline{r},\underline{n},t)$$

$$+ \frac{\beta(\underline{r},t)}{4\pi}\int_{4\pi} d\omega_{\underline{n}'}\, \chi(\underline{n}\cdot\underline{n}')\, J(\underline{r},\underline{n}',t) + S_0(\underline{r},\underline{n},t) \quad , \quad (1)$$

where J is the power radiated into direction $\underline{n}$ at location $\underline{r}$ at time t, ε is the extinction coefficient, β is the scattering coefficient and S_0 is a source term. The solid angle integration is carried out over the scattering phase function χ which represents the relative power scattered into direction $\underline{n}\cdot\underline{n}'$. To solve Eq. (1) define[8]

$$\alpha(\underline{r},t) = \frac{\beta(\underline{r},t)}{\varepsilon(\underline{r},t)} \leq 1$$

and set

$$J(\underline{r},\underline{n},t) = \sum_{k=0}^{\infty} [\alpha(\underline{r},t)]^k\, J_k(\underline{r},\underline{n},t) \quad . \qquad (2)$$

Substitution into Eq. (1) produces the coupled set of equations

$$\frac{1}{c}\frac{\partial J_k}{\partial t} + \underline{n}\cdot\nabla_{\underline{r}} J_k + \varepsilon(\underline{r},\underline{t}) J_k = S_k(\underline{r},\underline{n},t) \tag{3}$$

where

$$S_k(\underline{r},\underline{n},t) = S_0(\underline{r},\underline{n},t) \ , \qquad k = 0$$

$$= \frac{\varepsilon(\underline{r},t)}{4\pi}\int_{4\pi} d\omega_{\underline{n}'}\ \chi(\underline{n}\cdot\underline{n}')\ J_{k-1}(\underline{r},\underline{n}',t) \ , \qquad k > 0 \ .$$

These equations can be solved iteratively using the input source function S_0. An equivalent procedure is to look for solutions of the form

$$J_k(\underline{r},\underline{n},t) = c\int_{-\infty}^{t} dt' \int d^3 r' \int_{4\pi} d\omega_{\underline{n}'}\ G_0(\underline{r},\underline{n},t;\ \underline{r}',\underline{n}',t')\ S_k(\underline{r}',\underline{n}',t') \ , \tag{4}$$

where G_0 is the Green's function or propagator for scattered radiation. Using the method of characteristics G_0 can be shown to be

$$G_0(\underline{r},\underline{n},t;\ \underline{r}',\underline{n}',t') = \exp\left[-c\int_{t'}^{t} d\tau\ \varepsilon(\underline{r}-\underline{n}c(t-\tau))\right]\delta^3(\underline{r}-\underline{r}' - \underline{n}c(t-t'))\ \delta^3(\underline{n}-\underline{n}') \ , \tag{5}$$

where we have assumed ε to be time independent (or slowly fluctuating over the radiation transit time). We now define G_k, the Green's function for k^{th} order scattered radiation, as

$$J_k(\underline{r},\underline{n},t) = c\int_{-\infty}^{t} dt' \int d^3 \underline{r}' \int_{4\pi} d\omega_{\underline{n}'}\ G_k(\underline{r},\underline{n},t;\ \underline{r}',\underline{n}',t')\ S_0(\underline{r}',\underline{n}',t') \ . \tag{6}$$

An expression for G_k can be found by substituting the definition of S_k into Eq. (4) and applying Eq. (6); the result is

$$G_k(\underline{r},\underline{n},t;\ \underline{r}',\underline{n}',t') = c\int_{t'}^{t} dt''\int d^3\, r''\int d\omega_{\underline{n}''}\ G_0(\underline{r},\underline{n},t;\ \underline{r}'',\underline{n}'',t'')$$

$$\times\ \frac{\varepsilon(\underline{r}'')}{4\pi}\int_{4\pi} d\omega_{\underline{n}'''}\ \chi(\underline{n}''\cdot\underline{n}''')\ G_{k-1}\ (\underline{r}'',\underline{n}''',t'';\ \underline{r}',\underline{n}',t')\ . \tag{7}$$

Thus, J_k can be computed as an integral over the arbitrary source distribution S_0 of G_k as given in Eq. (7) in terms of lower order G_k's. Since the G's are independent of the source distribution, the problem has formally been solved for arbitrary S_0.

As an example of using Eq. (7) we find for G_1

$$G_1(\underline{r},\underline{n},t;\ \underline{r}',\underline{n}',t') = \frac{c}{4\pi}\ \chi(\underline{n}\cdot\underline{n}')\int_{t'}^{t} dt''\ T_1(t,t'')\ \varepsilon(\underline{r}-\underline{n}c(t-t''))$$

$$\times\ T_2(t'',t')\ \delta^3(\underline{r}-\underline{r}' - \underline{n}c(t-t'') - \underline{n}'c(t''-t')), \tag{8}$$

where

$$T_1(t,t'') \equiv \exp\left[-c\int_{t''}^{t} d\tau\ \varepsilon(\underline{r}-\underline{n}c(t-\tau))\right]$$

$$T_2(t'',t') \equiv \exp\left[-c\int_{t'}^{t''} d\tau\ \varepsilon(\underline{r}'+\underline{n}'c(\tau-t'))\right].$$

Equation (8) can be simplified substantially in the case of a uniform medium: namely

$$G_1(\underline{r},\underline{n},t;\ \underline{r}',\underline{n}',t') \xrightarrow[\text{medium}]{\text{uniform}}$$

$$c\ \varepsilon\ \frac{\chi(\underline{n}\cdot\underline{n}')}{4\pi}\ e^{-\varepsilon c(t-t')}\int_{t'}^{t} dt''\ \delta^3(\underline{r}-\underline{r}' - \underline{n}c(t-t'') - \underline{n}'c(t''-t'))$$

$$= c\varepsilon\ \frac{\chi(\underline{n}\cdot\underline{n}')}{4\pi}\ e^{-\varepsilon c(t-t')}\ \frac{\delta^2(\underline{\rho}-\underline{\rho}' - \underline{n}_\perp\ c(t-t_o) - \underline{n}_\perp'c(t_o-t'))}{|n_3' - n_3|} \tag{9}$$

where

$$t_0 \equiv \frac{z-z' - n_3\ ct + n_3'\ ct'}{c(n_3' - n_3)}$$

and

$$\underline{r} = (\underline{\rho}, z) \quad , \qquad \underline{n} = (\underline{n}_\perp, n_3) \quad .$$

2.2 Application to Backscatter

Equations 6 and 7 allow the radiance to be computed formally by orders of scattering for arbitrary source functions and spatial distributions of scatterers. In practice simplifying assumptions are needed to reduce the complexity of the required integrations. In this section we construct an expression for the first order backscatter power $P_1(t)$ by assuming 1) the small angle approximation and 2) the collection aperture and bistatic offset in the receiving plane as well as the field-of-view can be approximated as Gaussian functions.

Specializing Eq. 8 to the backscatter case ($z = z' = 0$) and performing the t" integration gives

$$G_1(\underline{\rho},\underline{n},t;\underline{\rho}',n',t') = \frac{c}{|n_3' - n_3|}\,\frac{\chi(\underline{n}\cdot\underline{n}')}{4\pi}\,\varepsilon(\underline{r} - \underline{n}c(t-t_0))\;T_1(t,t_0)\;T_2(t_0,t')$$

$$\times\;\delta^2(\underline{\rho} - \underline{\rho}' - \underline{n}_\perp c(t - t_0) - \underline{n}_\perp' c(t_0 - t')) \qquad (10)$$

where

$$t_0 \equiv \frac{n_3 t - n_3' t'}{n_3 - n_3'} \quad .$$

For the applications in mind the lidar transmitter beam divergence and receiver field-of-view angles are small ($\sim$ milliradians). This justifies making the small angle approximation $\underline{n}_\perp \cong \underline{\theta}$, $\underline{n}_\perp' \cong \underline{\theta}'$. This gives $t_0 \simeq (t + t')/2$.

Also,

$$T_1(t,t_0) \simeq \exp\left[-c\int_{\frac{t+t'}{2}}^{t} d\tau\,\varepsilon(\underline{r} - \underline{n}\; c(t-\tau))\right]$$

$$= \exp\left[-c\int_{t'}^{\frac{t+t'}{2}} d\tau\,\varepsilon(\underline{r}' + \underline{n}' c(\tau - t'))\right]$$

$$\simeq T_2(t_0,\; t')$$

and

$$G_1(\underline{\rho},\underline{n},t;\underline{\rho}',\underline{n}',t') \simeq \frac{c}{2}\,\frac{\chi(-1)}{4\pi}\,\varepsilon\left(\underline{\rho}' + \underline{n}'\; c\frac{(t - t')}{2}\right)\left[T_2(t_0,t')\right]^2$$

$$\times\; \delta^2\left(\underline{\rho} - \underline{\rho}' - (\underline{\theta} + \underline{\theta}')\; c\frac{(t - t')}{2}\right)\; . \qquad (11)$$

The power collected by a Gaussian field-of-view half angle θ_R with a Gaussian aperture radius a_R and bistatic offset $\underline{b}$ is

$$P_1(t) = \alpha\int d^2\underline{\rho}\; e^{-(\underline{\rho} - \underline{b})^2/a_R^2} \int d^2\underline{\theta}\; e^{-\theta^2/\theta_R^2}\; J_1(\underline{\rho},\underline{n},t) \qquad (12)$$

where the small angle approximation has been made for the field of view integration. Applying Eq. 6 and interchanging the orders of integration produces

$$P_1(t) = c\int_{-\infty}^{t} dt' \int d^2\underline{\rho}' \int d^2\underline{\theta}'\;\; S_0(\underline{\rho}',\underline{\theta}',t')\; p_1(\underline{\rho}',\underline{\theta}',t') \qquad (13)$$

with

$$P_1(\underline{\rho}',\underline{\theta}',t') = \alpha\int d^2\underline{\rho}\; e^{-(\underline{\rho}-\underline{b})^2/a_R^2}\int d^2\underline{\theta}\; e^{-\theta^2/\theta_R^2}\; G_1(\underline{\rho},\underline{n},t;\,\underline{\rho}',\underline{n}',t'). \quad (14)$$

Substitution of Eq. 11 gives

$$P_1(\underline{\rho}',\underline{\theta}',t') = \frac{c}{2}\,\frac{\chi(-1)}{4\pi}\,\beta\left(\underline{\rho}' + \underline{\theta}'\; c\frac{(t-t')}{2}\right)\left[T_2(t_o,t')\right]^2$$
$$\times \int d^2\underline{\theta}\; e^{-\theta^2/\theta_R^2}\quad \exp\left[-\left(\underline{\rho}_o + \underline{\theta}\; c\frac{(t-t')}{2}\right)^2\Big/a_R^2\right] \qquad (15)$$

where

$$\underline{\rho}_0 \equiv \underline{\rho}' + \underline{\theta}'\; c\frac{(t-t')}{2} - \underline{b}\quad .$$

Performing the integral gives

$$P_1(\underline{\rho}',\underline{\theta}',t') = \frac{c}{2}\,\frac{\chi(-1)}{4\pi}\,\beta\left(\underline{\rho}' + \underline{\theta}'\; c\frac{(t-t')}{2}\right)\left[T_2(t_0,t')\right]^2$$
$$\times \frac{\pi a_R^2\,\theta_R^2}{a_R^2 + \theta_R^2\left(c\frac{(t-t')}{2}\right)^2}\quad \exp\left[-\frac{\rho_0^2}{a_R^2 + \theta_R^2\left(c\frac{(t-t')}{2}\right)^2}\right]. \quad (16)$$

Equation 13 with 16 produces the desired expression for $P_1(t)$:

$$P_1(t) = \frac{c^2}{8}\,\chi(-1)\; a_R^2\,\theta_R^2\int_{-\infty}^{t} dt'\int d^2\underline{\rho}'\int d^2\underline{\theta}'\; S_0(\underline{\rho}',\underline{\theta}',t')\;\beta\left(\underline{\rho}' + \underline{\theta}'\; c\frac{(t-t')}{2}\right)$$
$$\times \frac{\left[T_2(t_0,t')\right]^2}{a_R^2 + \theta_R^2\left[c\frac{(t-t')}{2}\right]^2}\quad \exp\left[-\frac{\left|\underline{\rho}' + \underline{\theta}'\; c\frac{(t-t')}{2} - \underline{b}\right|^2}{a_R^2 + \theta_R^2\left[c\frac{(t-t')}{2}\right]^2}\right]\quad . \qquad (17)$$

2.3 Coherent trarsmitter example

We apply the first order power expression Eq. 17 to the case of a narrow coherent Gaussian transmitter beam. As examples we construct analytic expressions for the power collected from a uniform medium, and present numerical results for a three dimensional Gaussian cloud.

Assume for the source function

$$S_0(\underline{\rho}',\underline{\theta}',t') = \frac{E(t')}{\pi a_T^2}\, e^{-\rho'^2/a_T^2}\, \delta^2(\underline{\theta}' + \underline{\rho}'/f) \tag{18}$$

where E(t') specifies the temporal shape of the pulse. Equation 18 represents a coherent Gaussian transmitter wavefront with 1/e amplitude a_T and focal length f. Substitution of Eq. 18 into 17 gives

$$P_1(t) = \frac{c^2}{8}\chi(-1)\frac{a_R^2\,\theta_R^2}{\pi a_T^2}\int_{-\infty}^{t} dt' \frac{E(t')}{a_R^2 + \theta_R^2\left[c\frac{(t-t')}{2}\right]^2}\int d^2\underline{\rho}'\, e^{-\rho'^2/a_T^2}$$

$$\times\ \beta\left(\underline{\rho}'\left(1 - c\frac{(t-t')}{2f}\right) + \underline{e}_3\, c\frac{(t-t')}{2}\right)\left[T(t,t')\right]^2$$

$$\times\ \exp\left[-\frac{\left|\underline{\rho}'\left(1 - c\frac{(t-t')}{2f}\right) - \underline{b}\right|^2}{a_R^2 + \theta_R^2\left[c\frac{(t-t')}{2}\right]^2}\right] \tag{19}$$

where

$$T(t,t') = \exp\left[-c\int_{t'}^{\frac{t+t'}{2}} d\tau\ \varepsilon\left(\underline{\rho}'\left(1 - c\frac{(\tau-t')}{f}\right) + \underline{e}_3\, c(\tau - t')\right)\right]\quad . \tag{20}$$

In general, for arbitrary $\varepsilon(\underline{r})$, Eq. 19 must be evaluated numerically. For the special case $\varepsilon(\underline{r}) = \varepsilon_0$, a constant, $P_1(t)$ becomes

$$P_1(t) = \frac{c^2}{8}\chi(-1)a_R^2\theta_R^2\beta_0\int_{-\infty}^{t}dt'\,\frac{E(t')\,e^{-\varepsilon_0 c(t-t')}}{a_R^2+\theta_R^2\left[c\frac{(t-t')}{2}\right]^2+a_T^2\gamma^2}$$

$$\times\exp\left[-\frac{b^2}{a_R^2+\theta_R^2\left[c\frac{(t-t')}{2}\right]^2+a_T^2\gamma^2}\right] \tag{21}$$

where

$$\gamma \equiv 1-\frac{c(t-t')}{2f} \quad \text{and} \quad \beta_0 \equiv \alpha\,\varepsilon_0 \quad .$$

By the changes of variables $\xi' \equiv c(t-t')$, $\xi \equiv ct$, Eq. 21 may be written as a convolution

$$P_1(\xi) = \int_0^{\infty}d\xi'\,E(\xi-\xi')\,P_{1\delta}(\xi') \tag{22}$$

where

$$P_{1\delta}(\xi) = \frac{c}{8}\chi(-1)\,\frac{a_R^2\,\theta_R^2\,\beta_0\,e^{-\varepsilon_0\xi}}{a_R^2+\theta_R^2\left(\frac{\xi}{2}\right)^2+a_T^2\left(1-\frac{\xi}{2f}\right)^2}$$

$$\times\exp\left[-\frac{b^2}{a_R^2+\theta_R^2\left(\frac{\xi}{2}\right)^2+a_T^2\left(1-\frac{\xi}{2f}\right)^2}\right] \tag{23}$$

is the impulse response corresponding to a delta pulse in time. The two limiting cases of $\xi \to 0$ and $\xi \gg f$, a_R are

$$P_{1\delta}(0) = \frac{c}{8} \frac{\chi(-1) a_R^2 \theta_R^2}{a_R^2 + a_T^2} \beta_0 \exp\left[-\frac{b^2}{a_R^2 + a_T^2}\right] \quad (24)$$

$$\lim_{\xi >> f, a_R} P_{1\delta}(\xi) = \frac{c}{8} \frac{\chi(-1) a_R^2 \theta_R^2 \beta_0 e^{-\varepsilon_0 \xi}}{(\theta_R^2 + \theta_T^2)(\frac{\xi}{2})^2} \exp\left[-\frac{b^2}{(\theta_R^2 + \theta_T^2)(\frac{\xi}{2})^2}\right] \quad (25)$$

with $\theta_T = -a_T/f$. Notice that Eq. 25 reduces to the usual lidar equation as $b \to 0$. Figure 1 plots log $[P_{1\delta}(\xi)\ e^{\varepsilon_0 \xi} / \frac{1}{8}\ c\chi(-1)\beta_0]$ versus $\xi = ct$ for various values of the offset b using $a_R = 10$ cm, $a_T = 1$ cm, $\theta_R = \theta_T = 10^{-3}$. The exponential offset term dominates until $\xi \sim 2\ b\sqrt{\theta_R^2 + \theta_T^2}$; for longer ξ the $1/\xi^2$ term dominates.

Although Equations 22 and 23 provide insight into the dependence of lidar signal on system parameters, they are not adequate to model the return from localized distributions of scatterers. For this reason a computer program was developed to perform the integrations in Eq. 19 for arbitrary pulse shapes and smoke/dust distributions. In addition, it is often useful to estimate the ability of a lidar to detect a target through an obscuring cloud. For simplicity we model an infinite Lambertian plate target with arbitrary tilt with respect to the transmitter beam axis. Appendix 1 derives the power returned from this target, and Figure 2 plots the relative received power versus time for a 20 nsec square pulse incident on the target at various tilt angles.

Figure 3 plots the returns from a 10.6 μm lidar of the target at normal incidence at 1 km range illuminated through a three dimensional Gaussian smoke cloud centered at $z_0 = .5$ km and having 1/e radius $\sigma = 50$ m.

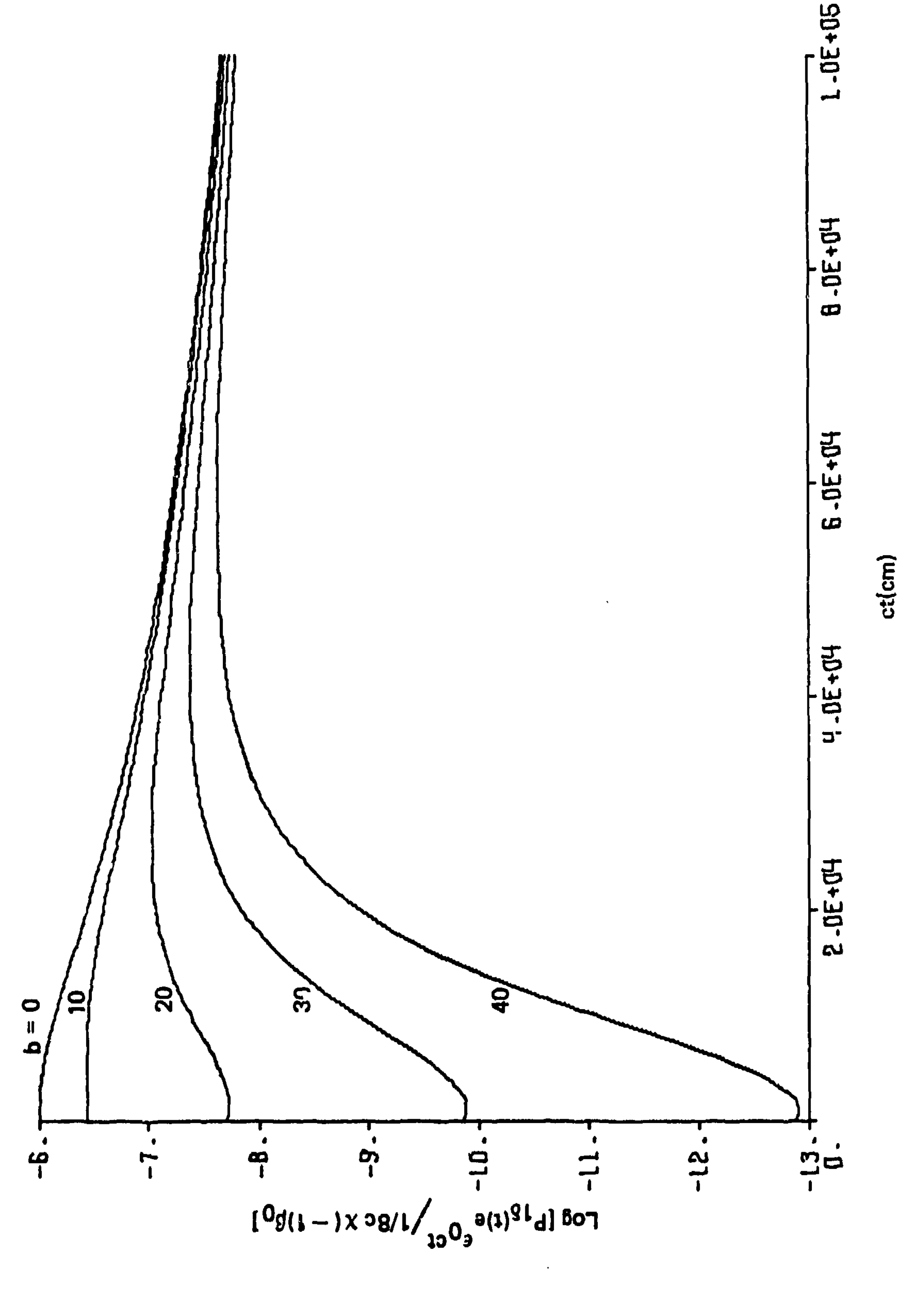

Figure 1. Normalized lidar return for various bistatic offsets.

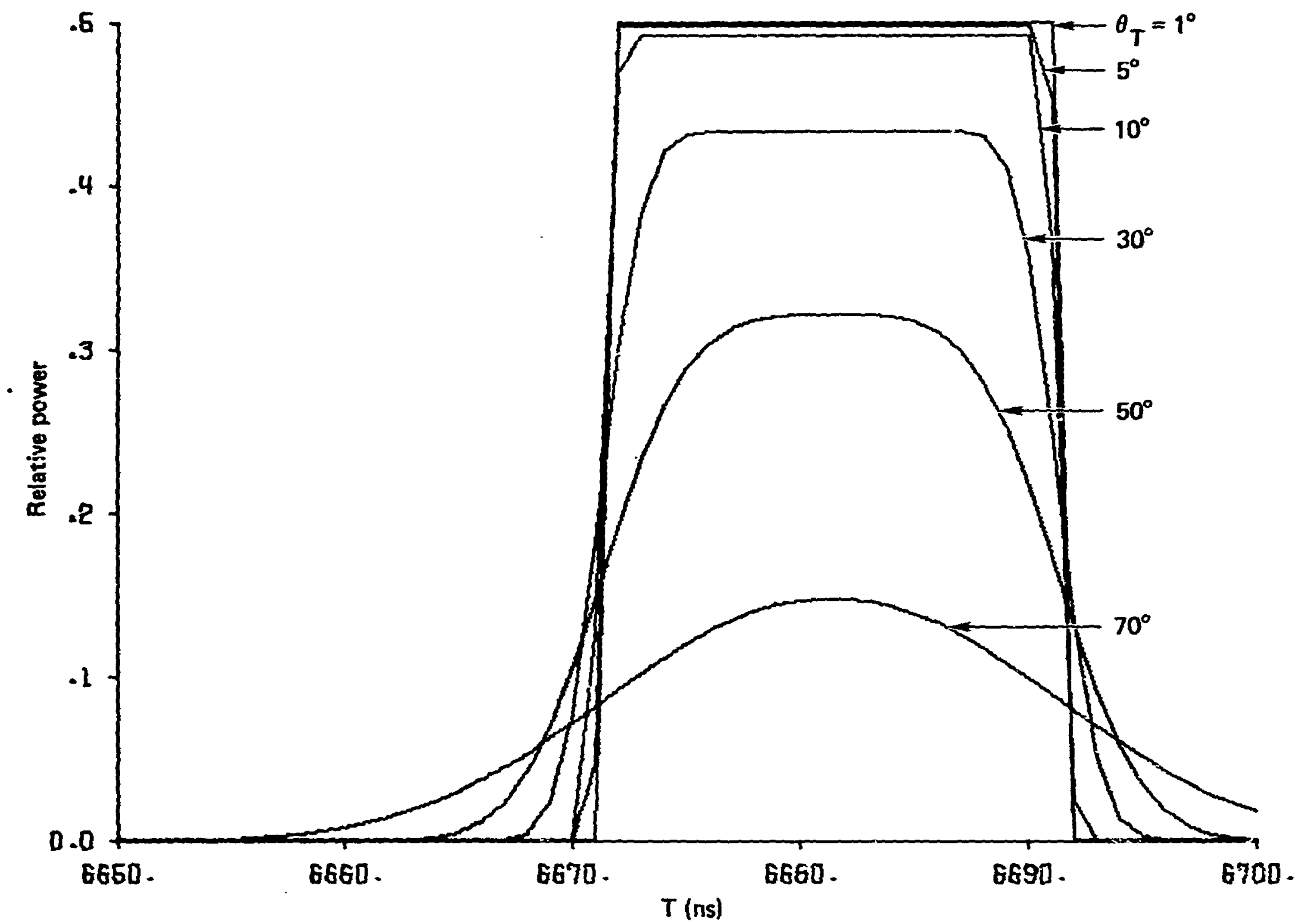

Figure 2. Received power from tilted Lambertian target.

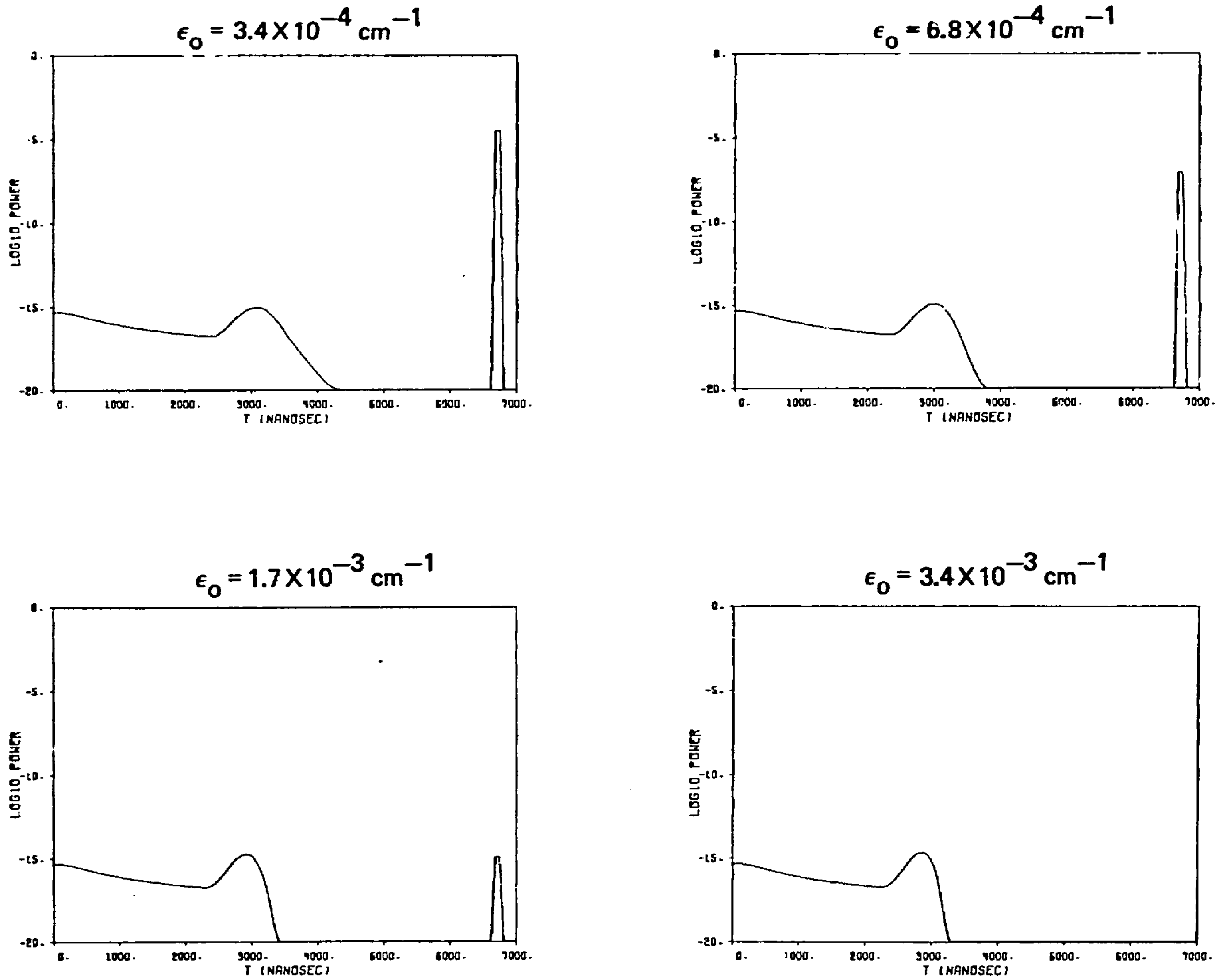

Figure 3. 10.6 µm lidar return from Lambertian target through Gaussian smoke clouds.

The extinction coefficient $\varepsilon(\underline{r})$ is taken to be

$$\varepsilon(\underline{r}) = \varepsilon_a + \varepsilon_0 \exp\left[-(\underline{r} - \underline{r}_0)^2/\sigma^2\right] \tag{26}$$

where $\underline{r}_0 = [0, 0, z_0]$ and ε_a is the ambient extinction. Table 1 summarizes the system and scattering medium parameters used in the computer calculation. The different plots in Figure 3 represent different values of ε_0, the peak extinction at the cloud center. Increasing ε_0 has the effect of reducing the target return and shifting the peak of the cloud return toward near ranges. This is due to the increased attenuation of the pulse as it penetrates the cloud center. For the case of largest ε_0 shown here the apparent cloud center is shifted from 500 m to about 435 m. This effect could have an important bearing on using lidar to map cloud concentrations.

Table 1

PARAMETERS USED IN LIDAR SAMPLE CALCULATION

Lidar System

Symbol	Meaning	Value
$P_1(t)$	1st order Lidar power	Computed
a_R	Receiver aperture radius	15 cm
θ_R	Receiver field-of-view 1/2 angle	2 mrad
b	Bistatic receiver offset	0
a_T	Transmitter aperture radius	3.1 cm
θ_T	Transmitter divergence 1/2 angle	1.2 mrad
f	Transmitter focal length	-2583.33 cm
E_0	Transmitter pulse energy	10^{-2}j
τ	Pulse duration	100 nsec

Medium

Symbol	Meaning	Value
α	Backscatter-to-extinction ratio	.001
ε_a	Ambient extinction	$0.2 \cdot 10^{-7}$ cm^{-1}
ε_0	Peak cloud extinction	3.4, 6.8, 17, 34 $\cdot$ 10^{-4} cm^{-1}
z_0	Cloud center	1 Km
σ	Cloud 1/e radius	50 m

3. METHODS OF ESTIMATING OBSCURANT CLOUD TRANSMISSIVITIES AND CONCENTRATIONS USING LIDAR.

3.1 Approach

One of the main goals of the present contract effort, namely the development of a mathematical lidar model with enough flexibility to analyze a broad range of systems and obscuring medium conditions, was addressed in the first part. It provides a framework for predicting the performance of a lidar system operating against three dimensional spatially varying obscurants. The other goal, that of defining a viable method of using a lidar to infer propagation path transmissivities and spatial concentrations of obscurants, will be addressed here.

There are two main applications for the data on obscuring clouds that can be derived from lidar. One use is to estimate the transmissivity between any point along the propagation path and the lidar system. This is of primary interest to those concerned with how well "observers" either human or electro-optical can see through battlefield obscurants. The other application is essentially that of using lidar as a diagnostic tool for mapping the spatial and time development of smoke and dust generated by explosive rounds. The first application is of more immediate tactical interest and is by far the simpler to achieve.

We first show that assuming the backscatter-to-extinction ratio α is approximately constant leads to a very simple means of estimating the path transmissivity from the lidar return if α itself can be estimated. The sensitivity of the proposed approach to uncertainties in α and system noise is then investigated, and a generalization of the approach using a point calibration measurement within the obscurant cloud is developed that would permit particle concentrations and "CL" values to be determined from the lidar as well as transmissivities. Finally, limited consideration is given to the possibility of using multiple wavelength systems to enhance the reliability and range of usefulness of lidar or as an alternative to the point calibration method.

3.2 Derivation of the Transmissivity Algorithm

Following the model results described in the first part, an approximate short pulse form of the lidar equation for a Gaussian aperture and field-of-view receiver is

$$P_1(t=2\frac{z}{c}) = \frac{A\ \beta(z)\ T^2(z)}{a_R^2 + \theta_R^2\ z^2 + (a_T + \theta_T z)^2}\ \exp\left[-\frac{b^2}{a_R^2 + \theta_R^2\ z^2 + (a_T + \theta_T z)^2}\right] \quad (27)$$

where

$$A \equiv \frac{c}{8}\ \chi(-1)\ a_R^2\ \theta_R^2\ E_0\ T_o \quad (28)$$

and

$$T(z) = \exp\left[-\int_0^z dz'\ \varepsilon(z')\right] \quad . \quad (29)$$

Eq. 27 results from Eq. 19 choosing

$$E(t) = \frac{E_0\ T_0}{c}\ \delta(t) \quad (30)$$

and approximating $\varepsilon(\underline{r}) \approx \varepsilon(\underline{e}_3 z)$ for $z = ct/2$. E_0 and T_0 represent the pulse energy and lidar system transmission. This equation can be integrated to find T(t) is we assume $\beta(z) \approx \alpha\ \varepsilon(z)$ over the propagation path; i.e., the backscatter is uniformly proportional to extinction. Since

$$\varepsilon(z)\ \exp\left[-2\int_0^z dt'\ \varepsilon(z')\right] = -1/2\ \frac{d}{dz}\ \exp\left[-2\int_0^z dz'\ \varepsilon(z')\right] \quad , \quad (31)$$

integration gives

$$T^2(z) = 1 - \frac{2}{A\alpha}\int_0^z dz'\; P_1\left(2\frac{z'}{c}\right)\left[a_R^2 + \theta_R^2\, z'^2 + (a_T + \theta_T z')^2\right]$$

$$\times \exp\left[\frac{b^2}{a_R^2 + \theta_R^2 z'^2 + (a_T + \theta_T z')^2}\right] \quad . \tag{32}$$

This result is essentially the same as Fernald et al.[9]

3.3 Sensitivity Analysis of the Transmissivity Algorithm.

Equation 32 allows the transmissivity to be estimated as a function of propagation range through the obscuring medium as an indefinite integral of the received lidar power. To make the idea practical several things are required:

1) It is necessary to have an accurate knowledge of the lidar system parameters. Note, however, the absolute value of the power collected does not need to be known because of the normalization A which includes the transmitted pulse energy; only the relative power received to that transmitted need be recorded.

2) Since the range and time resolution are related as $\Delta t = 2\Delta z/c$, 100 ft. range resolution requires 200 ns resolution in the recorded lidar signal; 10 ft. would require 20 ns resolution. This necessitates a short time response detector and high bandwidth recording system.

3) Eq. 32 requires an estimate of the backscatter-to-extinction ratio α be made. Since this is often poorly known, it is essential to understand the effect of uncertainties in α on the inferred transmissivity.

By differentiating Eq. 32 with respect to α, it follows

$$\frac{\Delta T}{T} = \frac{\Delta\alpha}{\alpha}\,\frac{1 - T^2}{2T^2} \quad . \tag{33}$$

Figure 4 plots this relation for various values of T. Clearly, the estimate of T is less sensitive to errors in α for larger T. The implication for using the technique on dense clouds is that an additional local measurement of α may be necessary.

In order to explore the effects of various uncertainties on the estimates of T using Eq. 32, a computer program was developed to compute the

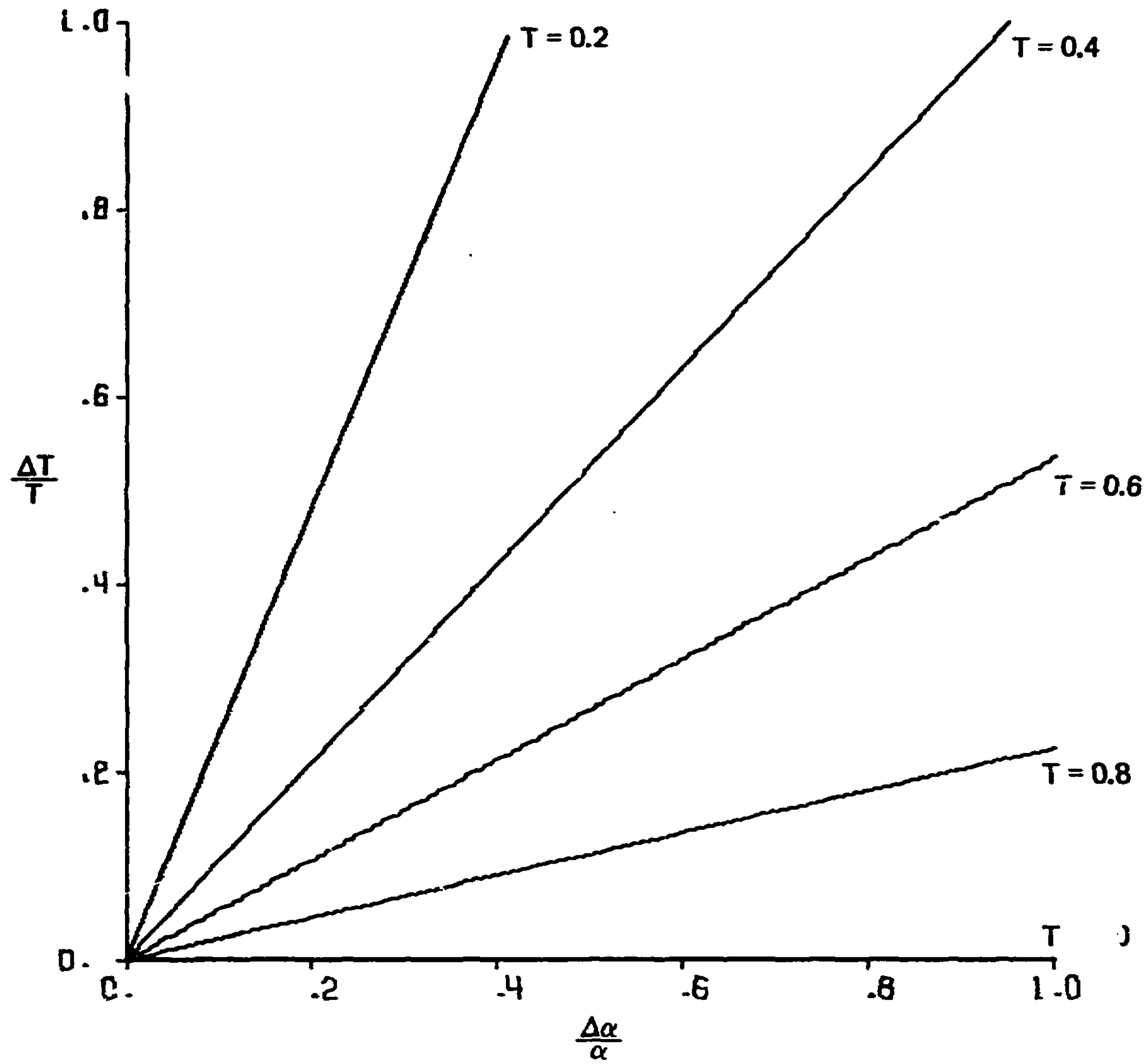

Figure 4. Effect of error in backscatter-extinction ratio on estimated transmission.

lidar power from Eq. 27, add Gaussian noise to simulate real-world conditions, and invert the signal plus noise with Eq. 32. The features we wished to investigate were the dependence of the computed transmissivity on noise, cloud density, and errors in α.

Figure 5 plots the theoretical lidar signal from a Gaussian cloud superimposed on the simulated signal with Gaussian noise chosen to represent a signal-to-noise ratio at the receiver ($z = 0$) of 100 (top) and 20 (bottom). The corresponding plots of theoretical and inferred transmissivity are shown to the right. The parameters are essentially the same as in Table 1 with $\varepsilon_0 = 2.5 \cdot 10^{-4}$ cm^{-1}.

Examination of the transmission curves shows the technique is capable of inferring the correct values for both SNR's up to the cloud center. Because of the strong signal attenuation from returns on the far side of the cloud, the inferred transmission estimates are unreliable for ranges greater than 1 km. Nevertheless, detailed inspection of the numerical computer output shows the technique can produce reasonably correct results for signals having only a SNR $\gtrsim$ .1; this results from the noise averaging produced by the integration.

In Figure 6 we compare the inferred transmission for two peak Gaussian cloud densities $\varepsilon_0 = 10^{-4}$ cm^{-1} (top) and $2.5 \cdot 10^{-4}$ cm^{-1} (bottom). The SNR at $z = 0$ was taken to be 100 in both cases. Increasing the cloud density by a factor of 2.5 causes drop outs in the inferred transmission for ranges greater than the cloud center; the technique works best for tenuous clouds.

Finally, we look again at the problem of uncertainties in the backscatter-to-extinction ratio α. Figure 7 shows the effect of producing simulated lidar signals and inverting them with 10, 20, and 50 percent

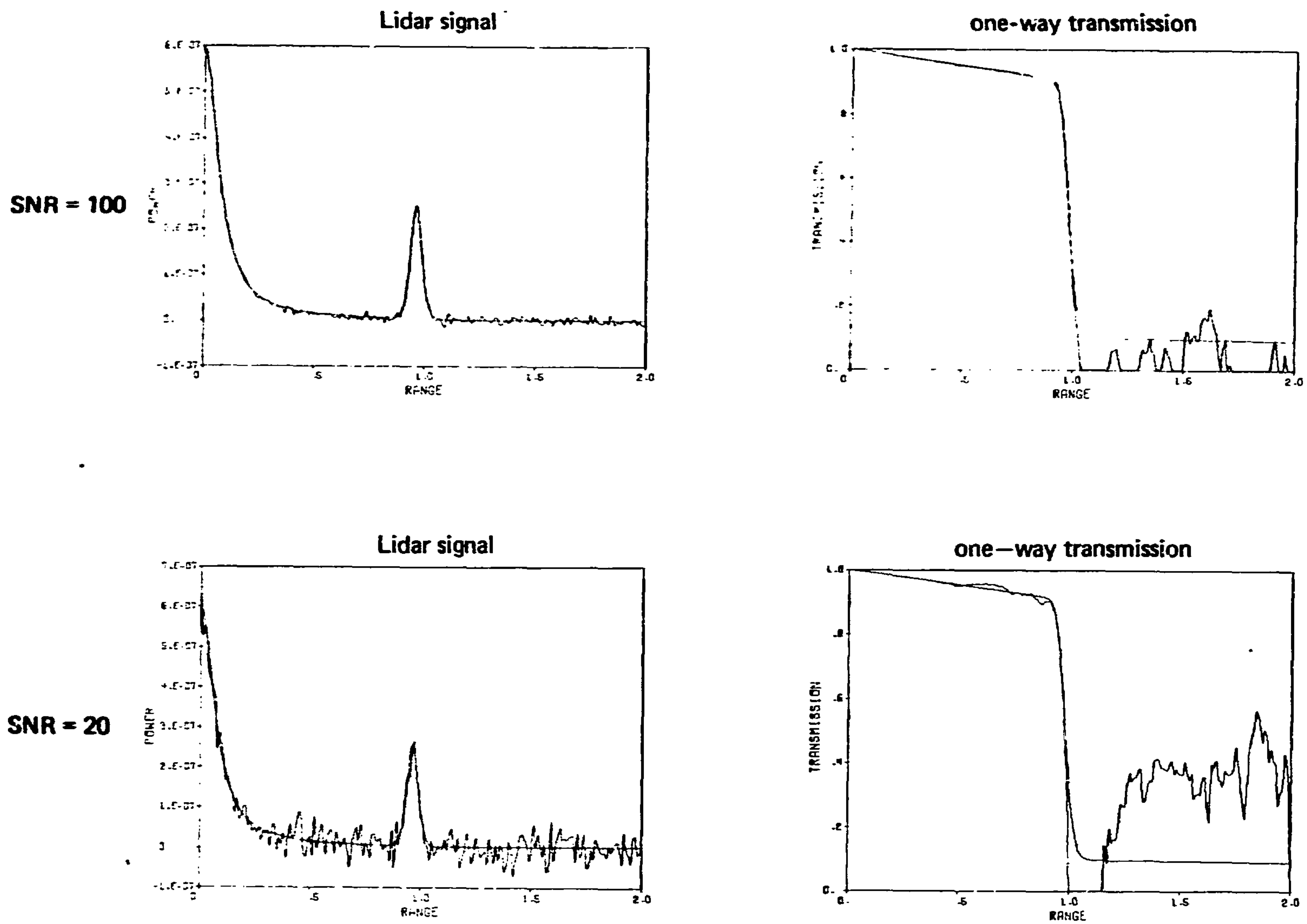

Figure 5. Sensitivity of lidar inversion to signal-to-noise ratio.

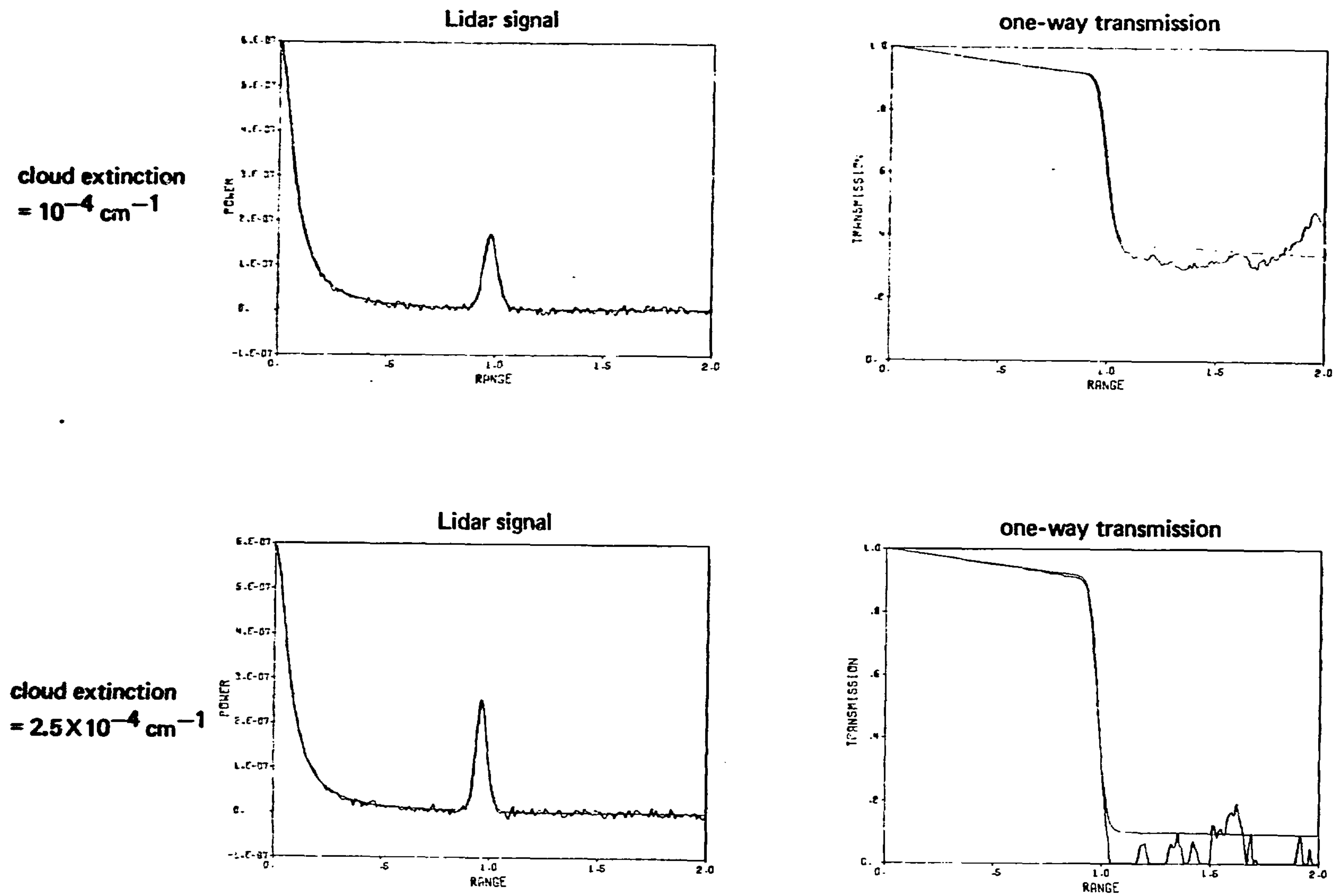

Figure 6. Sensitivity of lidar inversion to cloud density.

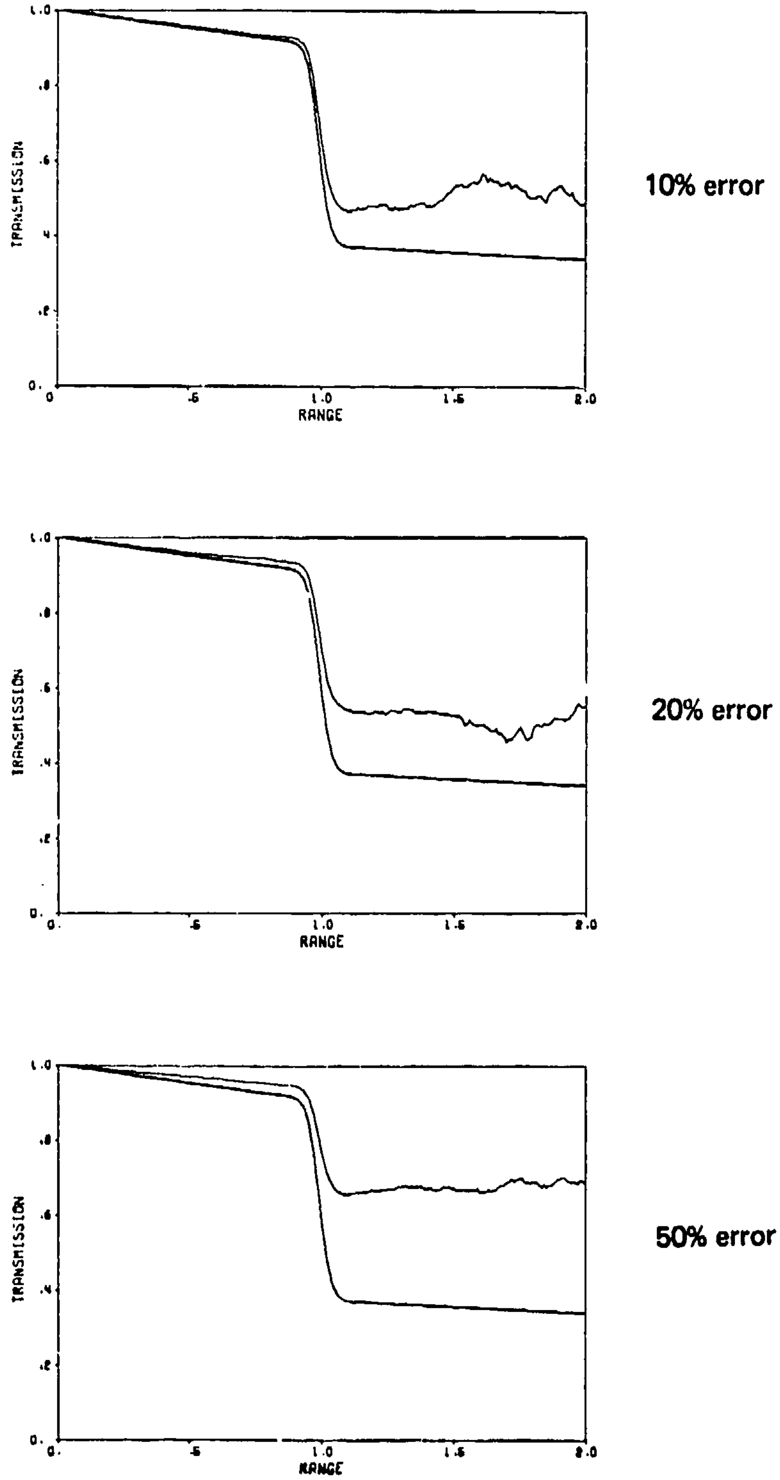

Figure 7. Sensitivity of lidar inversion to uncertainty in backscatter-extinction ratio.

errors in assumed α. For these runs $\varepsilon_0 = 10^{-4}$ cm^{-1} and SNR = 100 at $z = 0$. There is comparatively little distortion in the inferred transmission for ranges less than 1 km even for a 50% error in α. On the far side of the cloud, however, a 10% error significantly distorts the inferred transmission. These results agree with earlier observations.

In conclusion, the proposed lidar inversion technique should be useful for relatively weak returns (SNR $\gtrsim$ .1) if the backscatter-to-extinction ratio α can be characterized accurately. Errors in α will become more important as the transmission decreases.

3.4 Estimating Obscurant Concentrations and CL Values.

The lidar inversion technique described previously for computing transmissivity requires an accurate estimate of the backscatter-to-extinction ratio α. While in simple cases α may be characterized by *a priori* measurements (e.g. predominately single constituent scattering from a known material) in general it may be necessary to perform a local measurement simultaneous with the lidar measurement. If this is possible, and if certain other parameters can be measured in a small region of the propagation path, there is the possibility of inferring the spatial concentration throughout the region of non-zero lidar return. The purpose of the analysis here is to define the additional local measurements needed to calculate the spatial concentration and CL values and estimate how well the technique would be expected to work with white phosphorus smoke using either a 1.06 μm or 10.6 μm lidar.

From Eq. 27, the extinction coefficient is given by

$$\varepsilon(z) = \frac{P_1(2\frac{z}{c})\ [a_R^2 + \theta_R^2 z^2 + (a_T + \theta_T z)^2]}{A\ \alpha\ T^2(z)} \times \exp\left[\frac{b^2}{a_R^2 + \theta_R^2 z^2 + (a_T + \theta_T z)^2}\right] \quad (34)$$

where T(z) is estimated from Eq. 32. To compute the concentration set

$$\varepsilon(z) = \int_0^\infty dr\ n(r,z)\ \sigma_{tot}(r) \quad (35)$$

$$C_g(z) = \rho_0 \int_0^\infty dr\ n(r,z) \left(\frac{4\pi}{3} r^3\right) \quad , \quad (36)$$

where $\sigma_{tot}(r)$ is the extinction cross section for particles of radius r and n(r,z) is the number of particles of radius r at range z per unit volume. Here ρ_0 is the density of the smoke or dust constituent, assumed to be approximately spherical in shape. Set N(z) equal to the total number of particles/volume:

$$N(z) = \int_0^\infty dr\, n(r,z) \tag{37}$$

Then

$$\varepsilon(z) = N(z) \langle \sigma_{tot} \rangle \tag{38}$$

$$C_g(z) = \rho_0\, N(z) \langle V_p \rangle \tag{39}$$

so

$$C_g(z) = \rho_0 \frac{\langle V_p \rangle}{\langle \sigma_{tot} \rangle} \varepsilon(z) \tag{40}$$

where $\langle \sigma_{tot} \rangle$ and $\langle V_p \rangle$ are the average extinction cross section and particle volume for the density function n(r,z). Finally,

$$\begin{aligned} CL(z) &= \int_0^z dz'\, C_g(z') \\ &= \rho_0 \frac{\langle V_p \rangle}{\langle \sigma_{tot} \rangle} \int_0^z dz'\, \varepsilon(z') \quad . \end{aligned} \tag{41}$$

Equations (40) and (41) allow CL and the concentration to be estimated using Eqs. (32) and (34).

Applying this model to lidar data requires estimates to be made in a localized region of the propagation path of ρ_0, α, $\langle V_p \rangle$ and $\langle \sigma_{tot} \rangle$. Since the material of the assumed single scattering component is presumably known, ρ_0 is known. From local scattering estimates, the backscatter-extinction ratio α can be estimated. The last quantities can be estimated from local measurements of $n(r,z_o)$ and $\sigma_{tot}(r)$. Table 2 summarizes the steps needed to estimate $C_g(z)$ and CL from the lidar data.

For the analysis here we used white phosphorus smoke for which ρ_0 = 1.8 g/cm^3. Using a mean particle radius of .57 µm gives $\langle V_p \rangle$ = .755 · 10^{-12} cm^3. For the average extinction cross section we used 10^{-8} cm^2 and 2.94 · 10^{-8} cm^3 at 10.6 µm and 1.06 µm, respectively. The smoke cloud was modeled as a three-dimensional Gaussian density centered at 1 km with a peak number density of 3.4 · 10^{-4} particles/cm^3 and a one-sigma of 50 m. The assumed lidar parameters are summarized in Table 3.

Figure 8 plots the theoretical and inferred CL and concentration values for the two different wavelength systems. The inferred values were computed from the equations above using simulated lidar returns with added Gaussian noise chosen to represent a NEP of 1.372 · 10^{-11} watts. (This works out to a SNR of 10^3 at the transmitter-receiver.) The dropouts in the 1.06 µm plots occur at points where the inferred transmission becomes negative due to the simulated noise. It is clear that the 10.6 µm system is preferable under the single scatterer conditions assumed here. More work is needed to examine the advantages of using both wavelengths for multiple constituent obscurants with broad range of particle sizes since 10.6 µm return may be too weak for reliable inversion of small particle returns, in which case the 1.06 µm lidar would be preferable.

TABLE 2. LOGICAL FLOW OF CALCULATION OF $C_g(z)$ AND CL USING LIDAR.

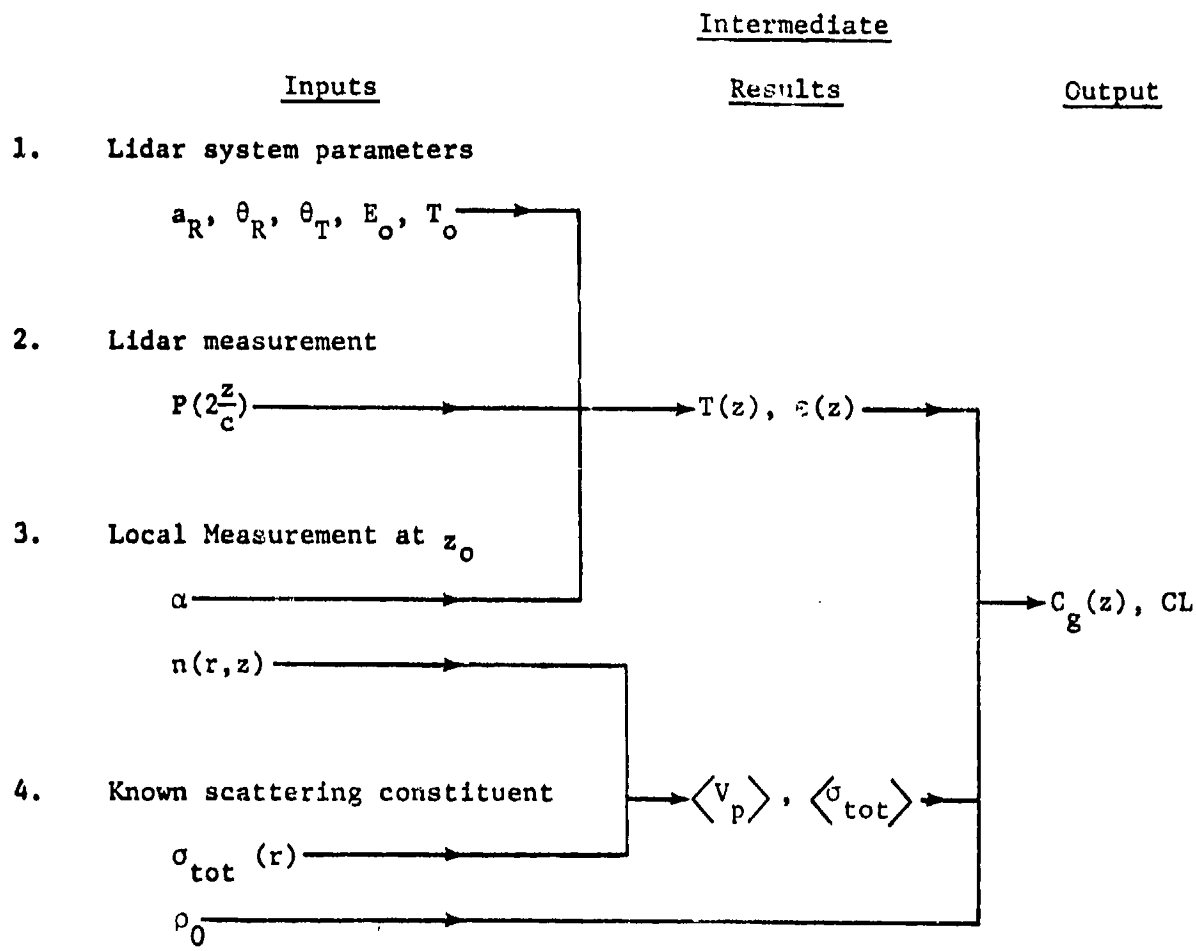

TABLE 3. SYMBOLS USED TO INFER CONCENTRATION FROM LIDAR

Lidar System

Symbol	Meaning	Values
P	Lidar return power	Computed
a_R	Receiver aperture radius	5. cm
θ_R	Receiver field of view ½ angle	.375 mrad
θ_T	Transmitter beam divergence ½ angle	.5 mrad
E_0	Transmitter pulse energy	10-2 j
T_0	Transmitter/receiver transmission	.45

Medium

$$\varepsilon(z) = \varepsilon_a + \varepsilon_0 \exp\left[-(z - z_0)^2/\sigma^2\right]$$

	10.6 μm	1.06 μm
ε_a	$0.2 \cdot 10^{-7}$ cm^{-1}	10^{-6} cm^{-1}
ε_0	$3.4 \cdot 10^{-4}$ cm^{-1}	10^{-3} cm^{-1}
α	.001	.001

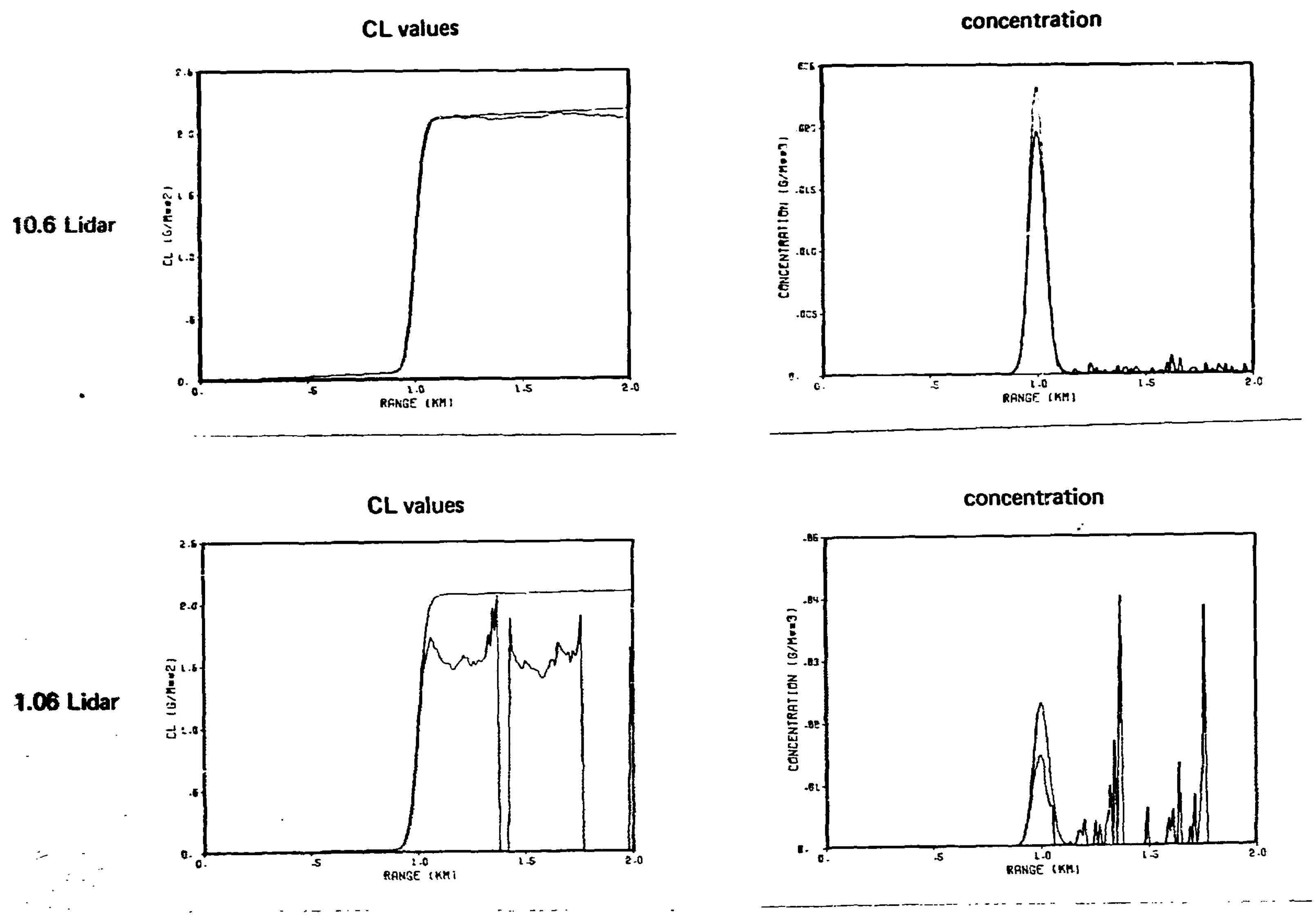

Figure 8. Theoretical and inferred CL values and concentrations for 10.6 μm and 1.06 μm lidars.

3.5 Multiple Wavelength Lidar

As stated previously, the utility of the proposed lidar inversion algorithm for estimating transmissivities and spatial concentrations is greatly enhanced by an auxiliary measurement of the backscatter-to-extinction ratio α. The last section outlined a technique incorporating a local measurement of scattering quantities including α to normalize the lidar signatures. For those cases where this direct measurement is infeasible some other method must be employed in general to estimate α. In this section we indicate a possible approach using a multiple wavelength lidar system.

If, instead of the single wavelength lidar, we have a number of simultaneous wavelength measurements, the backscatter coefficient for wavelength λ at range z becomes

$$\beta_\lambda(z) = \frac{P_{1\lambda}(2\frac{z}{c})\left[a_R^2 + \theta_R^2 z^2 + (a_T + \theta_T z)^2\right]}{A\, T_\lambda^2(z)} \times \exp\left[\frac{b^2}{a_R^2 + \theta_R^2 z^2 + (a_T + \theta_T z)^2}\right] \tag{42}$$

where T_λ^2 is computed from the analogous wavelength dependent version of Eq. 32 and an approximate estimate of α.

We now model $\beta_\lambda(z)$ as

$$\beta_\lambda(z) = \int_0^\infty dr\; n(r,z)\, \frac{d\sigma_a}{d\Omega}(\lambda,r,\pi) \tag{43}$$

where n(r,z) is the number of particles of radius r at range z per unit volume and $d\sigma_a/d\Omega$ is the differential backscattering cross section for particles of radius r (assumed spherical here) at wavelength λ. Equation 43 constitutes an integral equation at each range z which can in principle be solved for n(r,z) using β_λ from Eq. 42.

If n(r,z) can be estimated from Eq. 43 the extinction coefficient $\varepsilon(z)$ can be computed using Eq. 35 and estimates of $\sigma_{tot}(r)$. From this the transmissivity, α, concentration, and CL values can be computed using the equations of the last section.

The requirements needed to solve Eq. 43 for n(r,z) are:

1) The kernel of the integral equation $d\sigma_a/d\Omega$ must be specified using either Mie theory or a statistical generalization to account for different particle shapes and species.

2) Enough wavelength measurements must be performed with high enough signal-to-noise ratio to provide sufficient degrees of freedom to attempt numerical inversion of Eq. 43. Both of these are very strong requirements and more study is necessary to determine if they are within the grasp of current theoretical and hardware capability.

4. SUMMARY AND CONCLUSIONS

The accomplishments under the present contract effort include

1. Development of a three dimensional model for computing the lidar return for multiple orders of scattering for arbitrary spatially varying media.

2. Computer implementation of 1. for the case of first order scatter of a coherent (Gaussian) transmitter beam with arbitrary divergence, a (Gaussian) aperture and arbitrary field-of-view receiver, and a diffuse reflecting target with arbitrary orientation relation to the incident radiation.

3. Derivation and sensitivity analysis of a means of computing battlefield transmission by integrating the collected lidar signal.

4. Analysis of a means for estimating spatial concentrations and CL values of battlefield obscurants using results of 3. and a local measurement of scattering parameters.

The motivation for constructing the lidar model was to provide a predictive tool simple enough to provide physical insight into the scattering and collection process yet general enough to treat a wide range of applications and model extensions without reformulating new equations from first principles.

The Green's function expansion for multiple orders of scattering of the radiance was the approach chosen since it incorporates most but not all of the possible physical effects of the problem. The phenomena it does not include are diffraction and polarization; it was felt that these effects are relatively unimportant in comparison with the task of including them properly. Emphasis was placed on the first order return since for typical smoke or dust clouds the backscatter-to-extinction ratio α is about .001. There are obscurants, however, which could conceivably be of tactical interest such as petroleum oil smoke which absorbs relatively little energy in the ir[10] and would require more than the first order term to model their return. In this case the general formalism presented for higher orders would be of more than academic interest.

The lidar model was applied to the inverse problem of inferring information about the scattering medium from the lidar return. We showed that the assumption of direct proportionality between backscatter and extinction leads to a simple integration of the first order lidar equation to give the path transmission. A sensitivity analysis of the technique showed it to be relatively insensitive to noise but, depending on the cloud density, quite sensitive to the assumed backscatter-to-extinction ratio. Under the assumption that a localized measurement of the obscuring medium parameters could be made simultaneous to the global lidar measurement, it was demonstrated that not only α and the transmission but spatial concentrations and CL values could be measured.

Finally, we examined briefly the possibility of using an alternative to the local measurement involving a multiple wavelength lidar. Clearly, it is preferable to perform a direct measurement of the scattering parameters when possible, and there are important questions remaining to be resolved before it can be said with confidence that the multiple wavelength approach can produce comparable results. These questions involve modeling the differential cross sections of the aerosols constituting the obscurant and examining the resulting wavelength sensitivity to see how many and which wavelength are required. Furthermore, multiple scattering components introduce substantial additional complications which must be overcome to make the multiple wavelength approach effective.

Appendix

LIDAR RETURN FROM FLAT LAMBERTIAN TARGET

Following the approach of section 1.1 we define a target Green's function in the small angle approximation for $z = z' = 0$ as

$$G_T(\underline{\rho},\underline{n},t;\underline{\rho}',\underline{n}',t') = \frac{c}{2}\,\chi_T(\underline{n}\cdot\underline{n}_T)\;\beta_T(\underline{\rho}' + \underline{n}'c(\frac{t-t'}{2}))$$

$$\times\, T^2\;\delta^2(\underline{\rho} - \underline{\rho}' - (\underline{\theta} + \underline{\theta}')\;c(t-t')/2) \qquad \text{A-1}$$

where $\underline{n}_T$ is the unit vector specifying the orientation of the target and β_T defines the target reflectance. The transmission T is given by

$$T = \exp\left[-c\int_{t'}^{(t+t')/2} d\tau\;\varepsilon(\underline{\rho}' + \underline{n}'\;c(\tau - t'))\right] \quad . \qquad \text{A-2}$$

For a Lambertian target the scattering function χ_T is

$$\chi_T(\underline{n}\cdot\underline{n}_T) = \frac{\cos(\underline{n}\cdot\underline{n}_T)}{\pi} \quad . \qquad \text{A-3}$$

We model the target as an infinite flat surface. The condition for β_T to be non-zero is that $\underline{\rho}' + \underline{n}'\;c(t-t')/2$ lie on the surface. This is expressed mathematically as

$$[\underline{\rho}' + \underline{n}'\;c(t-t')/2 - \underline{r}_T]\cdot\underline{n}_T = 0 \qquad \text{A-4}$$

where $\underline{r}_T = [0,\,0,\,z_T]$ is the vector to the intersection of the plate and the z axis. Solving for $\xi_T \equiv c(t-t')$

$$\xi_T = 2(\underline{r}_T - \underline{\rho}') \cdot \underline{n}_T / (\underline{n}' \cdot \underline{n}_T) \qquad \text{A-5}$$

and

$$\beta_T = \beta_{T_0} \; \delta(\xi_T - c(t - t')) \quad . \qquad \text{A-6}$$

Proceeding as in section 1, we define a transmitter source function using Eq. 18 and compute the target radiance at the receiver

$$J_T(\underline{r},\underline{n},t) = c\int_{-\infty}^{t} dt' \int d^2\underline{\rho}' \int d\omega_{\underline{n}'} \; G_T(\underline{\rho},\underline{n},t;\underline{\rho}',\underline{n}',t') \; S_0(\underline{\rho}',\underline{n}',t')$$

$$= \frac{c}{2}\chi_T(\underline{n} \cdot \underline{n}_T) \; \beta_{T_0} \; T^2 \, \frac{E(t - \xi_T/c)}{\pi \, a_T^2 \, \gamma^2} \; \exp\left[-(\underline{\rho} - \underline{\theta}\xi_T/2)^2/\gamma^2 a_T^2\right] \qquad \text{A-7}$$

where

$$\xi_T = 2[\underline{\rho} - \underline{r}_T] \cdot \underline{n}_T / (\underline{n} \cdot \underline{n}_T) \qquad \text{A-8}$$

and

$$\gamma = 1 - \xi_T/2f \quad . \qquad \text{A-9}$$

The transmission is approximately

$$T \simeq \exp\left[-\int_{z_T}^{\xi_T} d\xi' \; \varepsilon(\underline{e}_3(\xi_T - \xi'))\right] \quad . \qquad \text{A-10}$$

For the target oriented perpendicular to the transmitter beam $\underline{n}_T = [0, 0, -1]$, $\xi_T = -2z_T/n_3 \simeq 2z_T$. Using Gaussian weighting functions for the receiver aperture and field-of-view

$$P_T(t) = \int d^2\underline{\rho}\; e^{-\rho^2/a_R^2} \int d^2\underline{\theta}\; e^{-\theta^2/\theta_R^2}\; J_T(\underline{r},\underline{n},t)$$

$$= \frac{c}{2}\,\frac{\beta_{T_0}}{\pi}\,T^2\,\frac{E(t - 2z_T/c)\;\pi a_R^2\theta_R^2}{a_R^2 + (a_T - \theta_T z_T)^2 + \theta_R^2 z_T^2} \qquad \text{A-11}$$

with

$$T = \exp\left[-\int_{z_T}^{2z_T} d\xi'\;\varepsilon(\underline{e}_3(2z_T - \xi'))\right] \quad . \qquad \text{A-12}$$

For non-zero target orientations, the integration of Eq. A-11 is much more difficult. The case of a square pulse can be integrated in closed form in terms of error integrals but more general cases require machine integration. Figure 2 plots the result for a 20 ns square pulse with various target orientations.

REFERENCES

1. E. D. Hinkley, *Laser Monitoring of the Atmosphere*, Springer, Berlin, 1976.

2. R. T. H. Collis and P. B. Russell, Chapter 4 in Ref. 1, 1976.

3. W. G. M. Blättner, *Feasibility Studies for the Use of Lidar for Measurements on Obscurant Clouds*, Final Report, RRA-77303, Radiation Research Associates, Fort Worth, Texas, 1978.

4. B. M. Herman, J. A. Reagan and R. M. Schotland, *A Feasibility Study on the Use of Lidar in the Determination of Optical Properties under Battlefield Conditions*, Final Report Contract DAAG-29-76-D-0100, University of Arizona, 1978.

5. E. E. Uthe, "Remote Sensing of Aerosol Properties Using Lasar Radar Techniques," *Optical Properties of the Atmosphere*, Vol. 142, SPIE, 1978.

6. E. E. Uthe, *Lidar Observations of Smoke and Dust Clouds at .7 μm and 10.6 μm Wavelengths*, SRI International, 1978.

7. C. W. Lamberts, *Lidar: A Statistical Approach*, Physics Laboratory of the National Defence Research Organization TNO, 1978.

8. A. M. Belyantsev, L. S. Dolin, and V. A. Savelev, "Propagation of Short-Duration Light Pulses in a Turbid Medium," *Izvestiya VUZ. Radiofizika*, Vol. 10, No. 4, 1967.

9. F. G. Fernald, B. M. Herman, and J. A. Reagan, "Determination of Aerosal Height Distributions by Lidar," *J. Appl. Meteor*, 11, 1972.

10. H. R. Carlon, D. H. Anderson, M. E. Milham, T. L. Tarnove, R. H. Frickel and I. Sindoni, "Infrared Extinction Spectra of some Common Liquid Aerosols," *Appl. Opt.* 16, 1977.